

Optical spectroscopy of bilayer graphene

Baisong Geng^{1,2}, Jason Horng¹, Yuanbo Zhang^{1,6}, Tsung-Ta Tang¹, Cheol-Hwan Park¹, Caglar Girit¹, Zhao Hao³, Michael Martin³, Alex Zettl^{1,4}, Michael Crommie^{1,4}, Steven Louie^{1,4}, and Feng Wang^{*,1,4}

¹Department of Physics, University of California, Berkeley, California 94720, USA

²School of Physical Science and Technology, Lanzhou University, Lanzhou 730000, China

³Advanced Light Source Division, Lawrence Berkeley National Laboratory, Berkeley, California 94720, USA

⁴Materials Science Division, Lawrence Berkeley National Laboratory, Berkeley, California 94720, USA

⁵Earth Sciences Division, Lawrence Berkeley National Laboratory, Berkeley, California 94720, USA

⁶Present address: Department of Physics, Fudan University, Shanghai 200433, China

Received 10 May 2010, revised 27 July 2010, accepted 5 August 2010

Published online 14 September 2010

Keywords bilayer graphene, Fano resonance, infrared spectroscopy, tunable bandgap

*Corresponding author: e-mail fengwang76@berkeley.edu, Phone: 1(510)643-3275, Fax: 1(510)643-8923

Infrared spectroscopy reveals unusual tunable electronic structure and optical behaviour in electrically gated bilayer graphene. In a dual-gate bilayer graphene device, we were able to control the carrier doping and a semiconductor bandgap independently by using different combinations of the top and bottom gate voltages. The field-induced bandgap can be probed directly through the emerging interband transitions in infrared absorption spectra. A tunable bandgap up to 250 meV has been observed in our dual-gate bilayer graphene devices. This unique tunable bandgap can lead to many new physical phenomena.

One example is an unusual phonon–exciton Fano resonance when the electronic bandgap is tuned to match the phonon vibration energy. Here (continuous) electron–hole transitions and (discrete) phonon vibrations form a coupled system described by the Fano resonance, and the infrared absorption spectra exhibit characteristic quantum interference between the phonon and exciton transitions. Remarkably, this coupled phonon–exciton Fano resonance can be continuously tuned through electrical gating in bilayer graphene, and its behaviour is described quantitatively by theory.

© 2010 WILEY-VCH Verlag GmbH & Co. KGaA, Weinheim

1 Introduction Graphene, a hexagonal sheet of carbon atoms, has attracted tremendous attention in the past few years because of its unique two-dimensional structure and the massless Dirac fermion-like charge carriers [1–5]. The electronic structure of two-dimensional graphene can be modified through electrical gating and layer–layer interactions. Such control is exemplified in bilayer graphene [6–9]. Interlayer couplings between AB-stacked graphene layers change the linear electronic structure in a monolayer to two parallel conduction bands and two parallel valence bands. Pristine bilayer graphene has the conduction and valence bands touching each other with a zero bandgap [10]. A finite bandgap can be induced in bilayer graphene by applying an external electrical field that breaks the inversion symmetry between the top and bottom graphene layers. This semiconductor bandgap can be continuously tuned through the applied electrical field strength [6, 7, 11].

Optical spectroscopy provides a powerful tool for probing the tunable physics in graphene. One major

breakthrough in graphene research is the realization of that a monolayer graphene can be seen with the naked eye under an optical microscope [12]. It indicates a very strong coupling between light and graphene, and photons can be a sensitive probe for electronic structures [10, 13–17], lattice vibrations [18] and carrier dynamics in graphene [19]. Here we use infrared spectroscopy to investigate the tunable electronic structure and optical transitions in dual-gated bilayer graphene. We demonstrate explicitly a tunable bandgap up to 200 meV through electrical gating. We also observe an unusual phonon–exciton Fano resonance in bilayer graphene resulted from resonantly coupled phonon and electron–hole pair excitations when the electronic bandgap is tuned to the phonon vibration energy.

2 Experiment and analysis We prepared bilayer graphene on the Si/SiO₂ wafer through mechanical exfoliation of kish graphite as described in Ref. [20]. Source and drain electrodes (Ti–Au of ~30 nm thickness) were

© 2010 WILEY-VCH Verlag GmbH & Co. KGaA, Weinheim

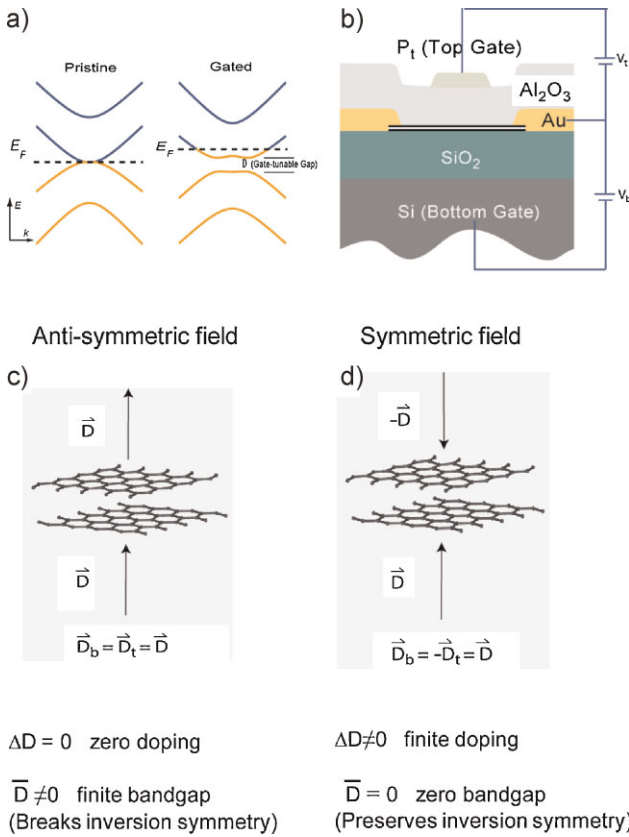


Figure 1 (online colour at: www.pss-b.com) Dual-gated bilayer graphene. (a) Pristine bilayer graphene has a zero bandgap (left). External electrical field can induce both carrier doping and a finite bandgap in bilayer (right). (b) An illustration of the side view of the dual-gate device. By controlling both electrical field above and below graphene, one can independently control the carrier doping and bandgap of bilayer graphene. A finite bandgap with zero carrier doping can be achieved with an anti-symmetric field, where $\Delta D = D_b - D_t = 0$ but $\bar{D} = (D_b + D_t)/2$ is finite (c). Finite carrier doping with a zero bandgap can be achieved with a symmetric field, where $\bar{D} = 0$ but ΔD is finite (d).

deposited directly on the graphene bilayer through a stencil mask in vacuum. The doped Si substrate under a 285-nm thick SiO₂ layer was used as the bottom gate. The top gate was made by sequential deposition of an 80-nm thick Al₂O₃ film and a semitransparent strip of Pt or ITO electrode. A side view of the dual-gate bilayer graphene device is illustrated in Fig. 1b.

A pristine AB-stacking bilayer graphene is undoped and has a zero bandgap protected by the inversion symmetry. Upon electrical gating, both the carrier concentration and semiconductor bandgap can be modified (Fig. 1a). The dual-gate configuration allows an independent control of the carrier doping and field-induced bandgap by applying suitable electrical field above and below the bilayer graphene. For example, an anti-symmetric field configuration breaks the inversion symmetry and creates a non-zero bandgap, but the continuity of the field above and below the graphene preserves the graphene charge neutrality (Fig. 1c).

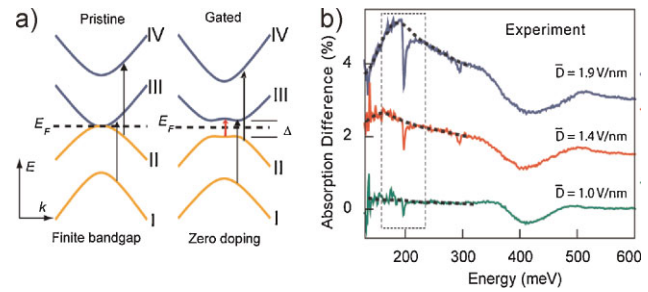


Figure 2 (online colour at: www.pss-b.com) A tunable non-zero bandgap opened by electrical gating. (a) Electron transitions between different bands in the bilayer graphene. Left, a pristine bilayer graphene has a zero bandgap. Right, a non-zero bandgap is induced by applied electric field. (b) Infrared absorption spectra of the gated graphene at CNPs with different electric displacement field \bar{D} . (The spectrum for zero bandgap CNP is subtracted as reference. The upper traces corresponding to 1.9 and 1.4 V/nm were displaced by 2 and 4% for clarity).

On the other hand, a symmetric field configuration in Fig. 1d generates electron doping in the bilayer graphene, but the bandgap remains zero because it preserves the inversion symmetry of the system. To achieve finite doping and bandgap opening, one can choose a suitable combination of the anti-symmetric and symmetric field. The bottom and top electrical displacement fields are determined separately by the top and bottom gated voltages in the form of $D_b = +\epsilon_b(V_b - V_b^0)/d_b$ and $D_t = -\epsilon_t(V_t - V_t^0)/d_t$. Here ϵ , d and V^0 are the dielectric constant, thickness of the dielectric layer and the effective offset voltage due to the initial induced carrier doping from environment.

We use infrared spectroscopy in a microscopy setup to measure the field-induced bandgap in bilayer graphene. We will focus on the anti-symmetric field configuration with zero carrier doping and a finite field-induced bandgap. Allowed optical transitions in pristine and gated bilayer graphene are depicted in Fig. 2a. In pristine bilayer graphene the main optical excitations are I → III and II → IV transitions. In gated bilayer graphene, the most striking difference is an emerging low energy transition from the valence band top to the conduction band bottom (II → III). In the meanwhile, I → III and II → IV transitions will also be modified. Figure 1b shows the experimental data for absorption difference between gated and pristine bilayer graphene at different applied average displacement electrical field \bar{D} . In the spectral range below 300 meV, a relatively broad absorption peak can be observed, which shifts to higher energy and becomes more prominent with strong electrical gating. (The sharp absorption dip is due to electron-phonon resonance, which we will examine later.) This absorption peak corresponds to the bandgap transition II → III. It increases from 150 to 190 meV when we tune the \bar{D} from 1.4 to 1.9 Vnm⁻¹. The enhancement of absorption intensity is due to the pile up of the density of the states at the band edge when we increase the bandgap. This observation provides direct evidence of a continuously tunable bandgap up to 200 meV in dual-gated bilayer graphene. The spectral

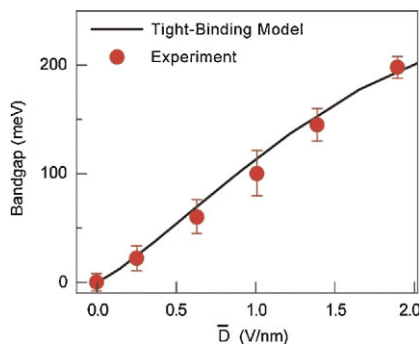


Figure 3 (online colour at: www.pss-b.com) Induced electronic bandgap in bilayer graphene as a function of applied displacement field. Red symbols are experimental data and the black line is from self-consistent tight-binding model.

feature around 400 meV corresponds to the I \rightarrow III and II \rightarrow IV transitions. In pristine graphene, this transition starts at 400 meV, but the absorption threshold for these transitions in gated bilayer graphene is shifted to higher energies due to bandgap opening. The difference spectra therefore exhibit an absorption dip at 400 meV due to a lack of absorption in gated sample at this energy and an absorption shoulder at slightly higher energy corresponding to the shifted absorption threshold upon gating.

We plot in Fig. 3 (red symbols) the induced bandgap energy as a function of applied average displacement electrical field. The bandgap increases monotonically with applied field strength. This behaviour is well-described by the self-consistent tight-binding theory using a graphene dielectric constant of 1 (black line) [7]. The maximum achievable bandgap in bilayer graphene is around 350 meV, limited by the layer–layer coupling strength. In our best sample, an induced bandgap of 250 meV has been observed.

This tunable bandgap in bilayer graphene is strikingly different from conventional materials where the bandgap is fixed by the material crystal structure. This unique ability to control the bandgap in bilayer graphene opens new possibilities in studying different physical phenomena. One example is the resonantly coupled phonon and electron–hole pair excitations, which is reflected in the sharp spectral features observed in Fig. 2.

The sharp spectral feature at 195 meV matches the G-mode phonon vibration frequency. However, instead of an absorption peak as one might expect, we observed an absorption minimum at the phonon resonance frequency. This unusual behaviour arises from quantum interference between resonantly coupled phonon and electron–hole excitations when the bandgap is close to the phonon vibration energy (Fig. 4). The coupled discrete phonon vibration and continuous electronic transitions form a characteristic Fano system with hybrid phonon–exciton excitation.

We examine next in detail how the phonon–exciton Fano resonance evolves as a function of electrical gating. We plot in Fig. 5 (black lines) the absorption spectra around 195 meV at different induced bandgaps in charge neutral bilayer

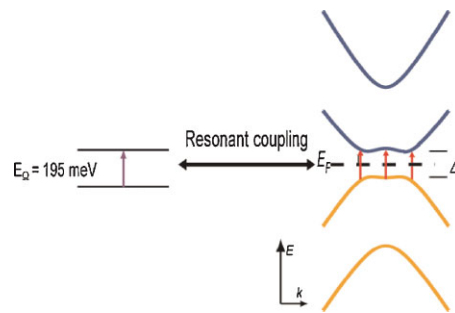


Figure 4 (online colour at: www.pss-b.com) An illustration of the Fano resonance in gated bilayer graphene. The phonon vibration couples with the electron transition resonantly and forms a Fano system.

graphene. In the analysis, we subtract the broad electronic absorption band from the measured spectrum to emphasize the sharp Fano resonance, which exhibits a significant lineshape change from a weak absorption dip to a dispersive interference, and to an absorption peak.

Fano resonance absorption has the form of

$$A - A_e = A_e \cdot \left(\frac{[q \cdot \Gamma + (E - E_\Omega)]^2}{(E - E_\Omega)^2 - \Gamma^2} - 1 \right),$$

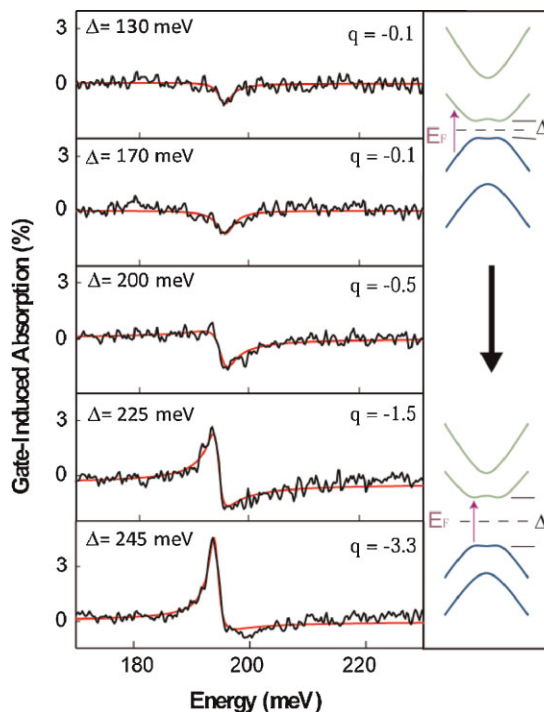


Figure 5 (online colour at: www.pss-b.com) Fano resonance absorption spectra of gated bilayer graphene. The black curves are experimental data with increasing field-induced bandgap from top to bottom. (The broad electronic absorption background has been subtracted.) The red curves are the Fano lineshape fitting, where the interference parameter q changes from $|q| \ll 1$ (phonon dominating) to $|q| \gg 1$ (electron dominating).

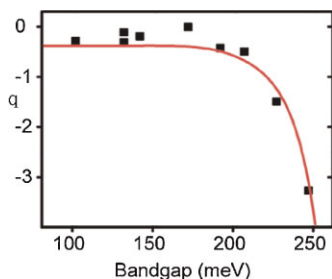


Figure 6 (online colour at: www.pss-b.com) The Fano parameter q as a function of the tunable bandgap in bilayer graphene at CNPs. The black square symbols are the fitted q value from experimental data and the red curve is the prediction from the theory.

where A is the absorption of graphene, A_e is the bare electronic state absorption, E_Ω and Γ are the centre energy and width of the phonon resonance, and the dimensionless parameter q characterizes the relative dipole strength of the renormalized phonon and electron transitions. At $|q| \ll 1$, electronic transition dominates and the absorption spectrum has a dip at the resonance; at $|q| \sim 1$, electronic and phonon absorption interference leads to a strongly dispersive lineshape; at $|q| \gg 1$ phonon absorption dominates and exhibits an absorption peak. Therefore, the evolution of Fano resonance lineshape in bilayer graphene can be qualitatively understood as an increasing Fano parameter at high electric field, and the optical transition at the resonance varies from mostly electronic to mostly phonon excitations.

Our observed tunable Fano resonances in bilayer graphene can be reproduced quantitatively by a second-order perturbation theory thanks to the simplicity of graphene phonon and electronic band structure. In bilayer graphene both symmetric and antisymmetric G-mode phonon exist. These two modes can intermix and both can contribute the electron–phonon Fano resonance in general. But with anti-symmetric field configuration as in our case, only symmetric phonon mode contributes to the Fano resonance. In Fig. 5, we fit the complete set of bilayer absorption spectra around 195 meV at different bandgap openings with the Fano lineshape (red lines), from which we obtain the Fano parameter q . With increasing gate electric field, q values change from -0.1 to -3.3 . Figure 6 plots the Fano parameter value obtained from the fitting as a function of the field-induced bandgap. They agree nicely with the theory prediction (red line).

3 Conclusions Our studies show that optical spectroscopy can be a valuable tool for probing the electronic structures and for revealing new excited state properties in graphene. In particular, optical transitions between the valence and conduction bands provide direct evidence of a large tunable bandgap in gated bilayer graphene. A bandgap opening as high as 200 meV was obtained with our dual-gate bilayer graphene device, which is much higher than the room temperature thermal energy. The tunable bandgap in bilayer

graphene also gives rise to a unique phonon–exciton Fano system that can be controlled through electrical gating.

Acknowledgements This work was supported by the University of California at Berkeley and the Office of Basic Energy Sciences, US Department of Energy under contract no. DE-AC03-76SF0098 (Materials Science Division) and contract no. DE-AC02-05CH11231 (Advanced Light Source). Y. Z. and F. W. acknowledge support from a Miller Fellowship and a Sloan Fellowship, respectively. T. T. T. is partially supported by the National Science Council, Taiwan.

References

- [1] M. I. Katsnelson, K. S. Novoselov, and A. K. Geim, *Nature Phys.* **2**, 620 (2006).
- [2] Y. Zhang, Y.-W. Tan, H. L. Stormer, and P. Kim, *Nature* **438**, 201 (2005).
- [3] A. K. Geim and K. S. Novoselov, *Nature Mater.* **6**, 183 (2007).
- [4] B. Huard, J. A. Sulpizio, N. Stander, K. Todd, B. Yang, and D. Goldhaber-Gordon, *Phys. Rev. Lett.* **98**, 236803 (2007).
- [5] K. S. Novoselov, A. K. Geim, S. V. Morozov, D. Jiang, M. I. Katsnelson, I. V. Grigorieva, S. V. Dubonos, and A. A. Firsov, *Nature* **438**, 197 (2005).
- [6] H. Min, B. Sahu, S. K. Banerjee, and A. H. MacDonald, *Phys. Rev. B* **75**, 155115 (2007).
- [7] E. McCann, *Phys. Rev. B* **74**, 161403 (2006).
- [8] F. Guinea, A. H. Castro Neto, and N. M. R. Peres, *Phys. Rev. B* **73**, 245426 (2006).
- [9] C. L. Lu, C. P. Chang, Y. C. Huang, R. B. Chen, and M. L. Lin, *Phys. Rev. B* **73**, 144427 (2006).
- [10] D. S. L. Abergel and V. I. Fal’ko, *Phys. Rev. B* **75**, 155430 (2007).
- [11] E. V. Castro, K. S. Novoselov, S. V. Morozov, N. M. R. Peres, J. M. B. L. dos Santos, J. Nilsson, F. Guinea, A. K. Geim, and A. H. C. Neto, *Phys. Rev. Lett.* **99**, 216802 (2007).
- [12] L. Gao, W. Ren, F. Li, and H.-M. Cheng, *ACS Nano* **2**, 1625 (2008).
- [13] F. Wang, Y. Zhang, C. Tian, C. Girit, A. Zettl, M. Crommie, and Y. R. Shen, *Science* **320**, 206 (2008).
- [14] A. B. Kuzmenko, E. van Heumen, D. van der Marel, P. Lerch, P. Blake, K. S. Novoselov, and A. K. Geim, *Phys. Rev. B* **79**, 115441 (2009).
- [15] K. F. Mak, M. Y. Sfeir, Y. Wu, C. H. Lui, J. A. Misewich, and T. F. Heinz, *Phys. Rev. Lett.* **101**, 196405 (2008).
- [16] J. Yan, E. A. Henriksen, P. Kim, and A. Pinczuk, *Phys. Rev. Lett.* **101**, 136804 (2008).
- [17] A. C. Ferrari, J. C. Meyer, V. Scardaci, C. Casiraghi, M. Lazzeri, F. Mauri, S. Piscanec, D. Jiang, K. S. Novoselov, S. Roth, and A. K. Geim, *Phys. Rev. Lett.* **97**, 187401 (2006).
- [18] J. Yan, Y. Zhang, P. Kim, and A. Pinczuk, *Phys. Rev. Lett.* **98**, 166802 (2007).
- [19] Z. Q. Li, E. A. Henriksen, Z. Jiang, Z. Hao, M. C. Martin, P. Kim, H. L. Stormer, and D. N. Basov, *Nature Phys.* **4**, 532 (2008).
- [20] K. S. Novoselov, D. Jiang, F. Schedin, T. J. Booth, V. V. Khotkevich, S. V. Morozov, and A. K. Geim, *Proc. Natl. Acad. Sci. USA* **102**, 10451 (2005).